Article

Rapid SNARE-Mediated Fusion of Liposomes and Chromaffin Granules with Giant Unilamellar Vesicles

Agata Witkowska[1,2] and Reinhard Jahn[1,*]

[1]Department of Neurobiology, Max-Planck-Institute for Biophysical Chemistry, Göttingen, Germany; and [2]International Max Planck Research School for Molecular Biology at the University of Göttingen, Göttingen, Germany

ABSTRACT   Soluble N-ethylmaleimide-sensitive factor activating protein receptor (SNARE) proteins are the main catalysts for membrane fusion in the secretory pathway of eukaryotic cells. In vitro, SNAREs are sufficient to mediate effective fusion of both native and artificial membranes. Here we have established, to our knowledge, a new platform for monitoring SNARE-mediated docking and fusion between giant unilamellar vesicles (GUVs) and smaller liposomes or purified secretory granules with high temporal and spatial resolution. Analysis of fusion is restricted to the free-standing part of the GUV-membrane exhibiting low curvature and a lack of surface contact, thus avoiding adhesion-mediated interference with the fusion reaction as in fusion with supported bilayers or surface-immobilized small vesicles. Our results show that liposomes and chromaffin granules fuse with GUVs containing activated SNAREs with only few milliseconds delay between docking and fusion. We conclude that after initial contact in *trans*, SNAREs alone can complete fusion at a rate close to fast neuronal exocytosis.

INTRODUCTION

Soluble N-ethylmaleimide-sensitive factor activating protein receptor (SNARE) proteins mediate most fusion events in the secretory pathway of eukaryotic cells (1,2). SNAREs are small and mostly membrane-anchored proteins that are distinguished by a stretch of 60–70 amino acids arranged in heptad repeats, referred to as the "SNARE motif". SNARE motifs can be classified into four evolutionarily conserved subfamilies. Fusion is mediated by the regulated assembly of four SNARE motifs, each belonging to a different subfamily. Assembly is thought to proceed from the membrane-distal N-terminal end of the SNARE motifs toward the membrane-proximal C terminus (zippering), a spontaneous and energy-releasing reaction resulting in a stable four-helix bundle. During zippering, the membranes are pulled tightly together, which ultimately causes fusion of the participating membranes (1). The SNAREs mediating Ca^{2+}-triggered exocytosis in neurons and neuroendocrine cells are particularly well studied. They include two SNAREs located at the plasma membrane (syntaxin 1A containing one SNARE-motif, and SNAP-25A with two SNARE-motifs), and one SNARE located at the vesicular membrane (synaptobrevin 2, also referred to as VAMP 2, with one SNARE-motif (3)). SNAREs are regulated by several accessory proteins including SM and CATCHR proteins responsible for initiating SNARE zippering, and synaptotagmins and complexins that only operate in Ca^{2+}-triggered exocytosis and are involved in triggering fusion (3,4).

Reconstitution of fusion with artificial membranes and purified proteins has been instrumental in furthering our understanding of SNARE-mediated fusion at the molecular level. A variety of different fusion assays has been developed over the last years that each have advantages and disadvantages. Initially, fusion was studied using two sets of small unilamellar vesicles (SUVs, 30–40 nm in diameter) containing either plasma membrane SNAREs or synaptobrevin, with lipid mixing being monitored by a reduction in fluorescence resonance energy transfer (FRET) due to the dilution of two labeled lipids during fusion (5). This assay is still widely used and has been modified in various ways. For instance, it was adapted to larger vesicles (to reduce curvature stress, for 100 nm vesicles, see, e.g., (6), for μm-size giant vesicles see e.g., (7,8)), to the measurement of content mixing (9), and it was further modified to allow for differentiating hemifusion from fusion (6,10). However, these assays all have limited kinetic resolution, particularly because it is difficult (although principally

---

CrossMark

possible, see (11)) to differentiate the initial binding of the fusion partners (docking) from fusion. Moreover, it is not possible to follow individual fusion events. To overcome these limitations, several microscopy-based assays were developed that involve immobilization of one of the membranes involved in the fusion reaction. Generally, two approaches are used—the first one involving planar, surface-supported or suspended bilayers (see, e.g., (12–16)), and the second one involving surface immobilization of small proteoliposomes with a size below the diffraction limit of the light microscope (see, e.g., (17–19)). In both approaches the surface-immobilized membranes are kept in the focal plane of the microscope, with vesicles then being added in solution, thus allowing for monitoring docking and fusion of single vesicles with high time resolution. Although these assays are versatile and are also widely used, surface-attachment of the membranes may result in nonspecific adhesion and the development of stress forces, which may affect and even compromise detection of the features of the fusion reaction.

Here our goal was to develop a system in which docking and fusion of single vesicles with a nonadherent membrane free of curvature stress can be monitored. To this end, we used giant unilamellar vesicles (GUVs) immobilized on the glass surface and smaller diffusing vesicles and monitored docking and fusion with a fast confocal microscope. With this system we have been able to obtain high temporal and spatial resolution (with millisecond kinetics) of single vesicle fusion events using both liposomes and purified secretory granules.

MATERIALS AND METHODS

Reagents

Oregon Green 488 and Texas Red (TR)-coupled DHPE were purchased from Invitrogen (Waltham, MA). Lipophilic tracers—DiO and DiD, Texas Red maleimide (for protein labeling), NeutrAvidin, and biotinylated bovine serum albumin—were from Thermo Fisher Scientific (Waltham, MA). Calcein, sulforhodamine B, and other chemicals were from Sigma-Aldrich (St. Louis, MO). All other lipids were purchased from Avanti Polar Lipids (Alabaster, AL): brain-PC (L-α-phosphatidylcholine (Brain, Porcine)), brain-PE (L-α-phosphatidylethanolamine (Brain, Porcine)), brain-PS (L-α-phosphatidylserine (Brain, Porcine)), cholesterol (ovine wool), 18:1 Biotinyl Cap PE (1,2-dioleoyl-sn-glycero-3-phosphoethanolamine-N-(cap biotinyl)), 18:1 NBD-PE (1,2-dioleoyl-sn-glycero-3-phosphoethanolamine-N-(7-nitro-2-1,3-benzoxadiazol-4-yl)), and 18:1 Liss Rho-PE (1,2-dioleoyl-sn-glycero-3-phosphoethanolamine-N-(lissamine rhodamine B sulfonyl)).

Protein purification and labeling

Constructs encoding SNARE proteins were derived from *Rattus norvegicus* and were expressed in *Escherichia coli* and purified with affinity and ion-exchange chromatography as described previously in Hernandez et al. (6) and Pobbati et al. (20). We used single cys mutant (C28) of synaptobrevin 1–116 (wild-type (WT) syb, (21)), a single deletion mutant Δ84 syb 1–116 (Δ84 syb; (6)), a short C-terminal fragment of syb 49–96, syntaxin 1A lacking the N-terminal Habc domain (183–288), and a cysteine-free variant of SNAP-25A in which a single cysteine mutation (C130, (21)) was introduced. Fluorescence labeling of proteins was carried out using Texas Red maleimide. ΔN SNARE acceptor complex consisting of syntaxin (183–288, (22)), SNAP-25A, and syb 49–96 (ΔN complex) was assembled from monomers and purified in *n*-octyl-β-D-glucopyranoside (GLYCON Biochemicals, Luckenwalde, Germany) as described in Pobbati et al. (20). Labeled complex was formed in the same way except for SNAP-25A that was replaced with a C130 mutant labeled with TR.

Liposome preparation

For all liposome mixtures PC, PE, PS, and cholesterol were mixed in a ratio of 5:2:2:1, respectively. Labeled lipids, biotinylated lipids, or lipophilic tracers were incorporated by replacing a portion of PC (or PE in the case of PE-labeled species) with usually 1 mol % of respective labeled molecule (1.5 mol % were used for NBD/Rhodamine FRET experiments; Fig. 2 *a*).

Large liposomes (large unilamellar vesicles (LUVs), diameter 100 nm) were prepared as described in Hernandez et al. (6) using reverse phase evaporation. Synaptobrevin was reconstituted in a protein/lipid of 1:500 using the direct reconstitution method as described in Hernandez et al. (6).

Small proteoliposomes (SUVs, diameter 40 nm) were prepared essentially as described in Pobbati et al. (20), except that the buffer was replaced with 20 mM HEPES/KOH pH 7.4 and 150 mM KCl (liposome buffer) containing 5% (w/v) sodium cholate if indicated. SUVs containing the SNARE acceptor complex were prepared to yield a protein/lipid of 1:1000 (1:200 for calcein content mixing, Fig. 2 *b*), and SUVs used for content mixing contained 200 mM calcein or 100 mM sulforhodamine B, and syb at a protein/lipid of 1:500.

GUV preparation

ΔN-GUVs (acceptor complex containing GUVs) were prepared largely following the protocol described in Bacia et al. (23), using a method known to yield mainly unilamellar vesicles (24). Briefly, SUVs containing acceptor complex and biotinylated-PE were dried on indium tin oxide-coated glasses (15–30 Ω; Diamond Coatings, Halesowen, United Kingdom) overnight in a desiccator. Afterwards, an electroformation chamber (consisting of two sandwiched indium tin oxide-glasses separated by a 3-mm-thick silicone spacer) was assembled and filled with 200 mM sucrose solution. Electroformation was performed by applying an alternating electric field (peak-to-peak) for 3 h (3.4 V, 10 Hz), followed by a detachment phase for ~1 h (3.4 V, 4 Hz). Finally, the chamber was disassembled, and the GUVs were collected for further experiments.

Microscopy imaging and analysis

Before each experiment, glass coverslips were coated with biotinylated BSA (2 mg/mL) for 1 h, and subsequently incubated with NeutrAvidin solution (0.7 mg/mL in liposome buffer, 1 h). 100–200 μL GUV solution was diluted with 300 μL liposome buffer containing 1 mM MgCl$_2$, introduced into an imaging chamber containing a coated coverslip on the bottom, and incubated for at least 30 min to allow the GUVs to settle and become immobilized. Liposomes or chromaffin granules were added before image acquisition to the imaging chamber with immobilized GUVs. GUVs that were not unilamellar (i.e., did not have uniform membrane fluorescence, showed a higher fluorescence intensity than other GUVs of similar size, or contained luminal inclusions) were excluded from image acquisition and data analysis. Images were primarily analyzed and normalized with the software Fiji (25), and are mostly shown with a fire lookup table (fluorescence intensity scale bar shown in Fig. 2 *a*).

Details of the microscope setups and settings are given in the Supporting Material (Tables S1 and S2).

Determination of the efficiency of GUV reconstitution

The concentration of ΔN complexes in the GUV membrane (C_{prot}) was determined as described in Aimon et al. (26) with some modifications, as follows:

$$C_{prot} = \frac{I_{mp}}{N_f \times M_{ref} \times F},$$

where I_{mp} is the membrane fluorescence intensity of the protein, N_f is the number of fluorescent dyes attached to one protein molecule, M_{ref} is a calibration factor, and F is the calibration scaling factor.

In this method, membrane fluorescence intensity of the TR-labeled complex was compared with that of a reference fluorophore (TR-PE), expressed with a calibration factor M_{ref}, as follows:

$$M_{ref} = \frac{\sum_{i=1}^{n} \frac{I_{ml}}{C_{ml}}(i)}{n},$$

which is calculated from a calibration curve (Fig. S2 a) generated from membrane fluorescence intensities (I_{ml}) of n-number of varying concentrations of TR-PE (C_{ml}).

Additionally, intrinsic properties of a dye attached to a molecule (protein or lipid) were taken into account, by scaling the calibration (M_{ref}) with a fluorescence intensity ratio F of a bulk, equimolar, detergent solution of labeled species, as follows:

$$F = \frac{I_{dp}}{I_{dl}},$$

where I_{dp} and I_{dl} are fluorescence intensities of detergent solutions of labeled protein and lipid, respectively.

Membrane fluorescence peak intensities (for Figs. 1 a, 2, a and b, and S2 a) were calculated using a self-written ImageJ macro that identifies GUV, linearizes membrane with a polar transformation method, and measures an average line peak intensity of a membrane (see Code Availability, GUV membrane linearization macro).

Fluorescence recovery after photobleaching analysis

For calculation of lipid and protein diffusion coefficients in a GUV membrane, fluorescence recovery after photobleaching (FRAP) experiments were performed. A circular bleach area was located on the top of the GUV (see (7,27)). Digitized fluorescence intensity data were normalized and analyzed with a self-written macro implementing data extraction from microscopy images in the software Fiji and automatic analysis in GNU Octave ((28); see Code Availability). Normalized data points were averaged for each group of GUVs with the same bleaching settings and coming from the same preparation, and fitted to the formula developed by Soumpasis (29), as shown here:

$$f(t) = Ae^{-\tau/2t}\left[I_0\left(\tau/2t\right) + I_1\left(\tau/2t\right)\right],$$

where I_0 is the modified Bessel function of the first kind of zero order, and I_1 is the modified Bessel function of the first kind of first order; A is the amplitude; t is time; and τ is the time constant. The diffusion coefficient D is calculated from the following equation:

$$D = \frac{r^2}{\tau},$$
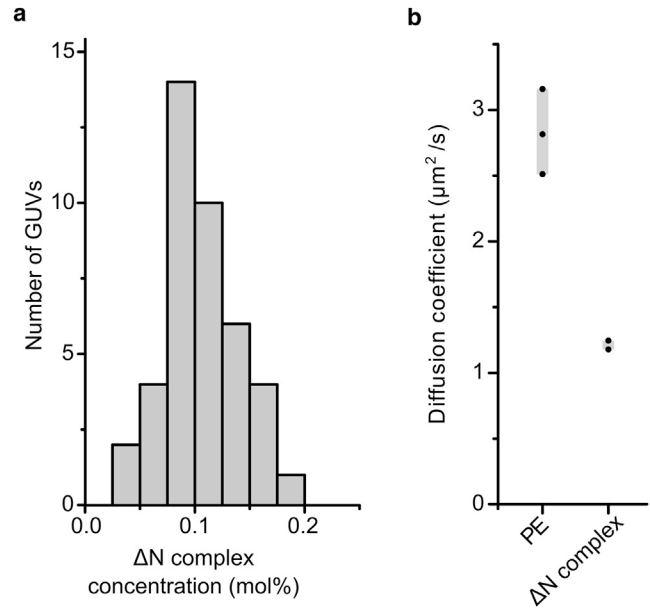
with r being the radius of the bleached spot.

FIGURE 1 Reconstitution of the SNARE acceptor complex into GUVs is highly efficient. (a) Histogram showing the distribution in the concentration of the acceptor complex in the membrane of GUVs ($n = 41$, bin size = 0.025 mol %) obtained by comparing membrane peak fluorescence intensity at the vesicle equator of GUVs containing labeled ΔN complex with GUVs containing known concentration of labeled lipid (TR-PE, for details see Materials and Methods). (b) Mobility of the SNARE acceptor complex, in the plane of the GUV membrane, in comparison to the mobility of membrane lipids. The diffusion coefficients were determined by performing FRAP measurements of TR-PE or TR-ΔN complex using bleaching of an area on the top of the GUVs. Dots represent mobilities obtained for groups of GUVs and gray bars represent range of obtained values ($n_{PE\_total} = 19$, $n_{\Delta N\_total} = 16$).

Lipid mixing

Bulk lipid mixing experiments involved GUVs containing 1.5 mol % NBD-PE and LUVs containing 1.5 mol % Rhodamine-PE. Upon vesicle fusion, FRET between these two labels occurs and thus NBD fluorescence is quenched. Based on the principle of acceptor photobleaching FRET microscopy (30), photobleaching of Rhodamine (FRET acceptor) in the equatorial plane of the GUV led to the recovery of NBD fluorescence.

In the case of single LUV to GUV fusion, a non-FRET pair of fluorescence labels was used (usually DiO and DiD), and fusion was identified by the diffusion of LUV label in the GUV membrane. Images were acquired as z-stacks (containing usually 3–4 planes separated by 0.3 μm) over time to capture events where vesicle docking was followed by diffusion on GUV membrane (in three dimensions). Such $xyzt$ image stacks were then treated as continuous time sequences and were searched for vesicle docking on the GUV membrane followed by fusion. Events where docking was followed by detachment or diffusion of a docked vesicle out of imaged volume were discarded (for examples of such events, see Fig. S6, b and c). Detection of fusion was additionally confirmed by analysis of line profiles that were extracted from a ~0.6-μm-thick region including linearized GUV membranes (linearization done with a polar transformation method; see Code Availability and Fig. S5). Images taken for line profiles were normalized by subtracting an averaged stack image from every time frame. For more detailed information about the analysis workflow, see Fig. S4.

Determination of fusion kinetics was done by fitting (Origin; OriginLab, Northampton, MA) of a cumulative frequency distribution of lag times between docking and fusion to a first-order kinetic equation as in Kiessling et al. (31).
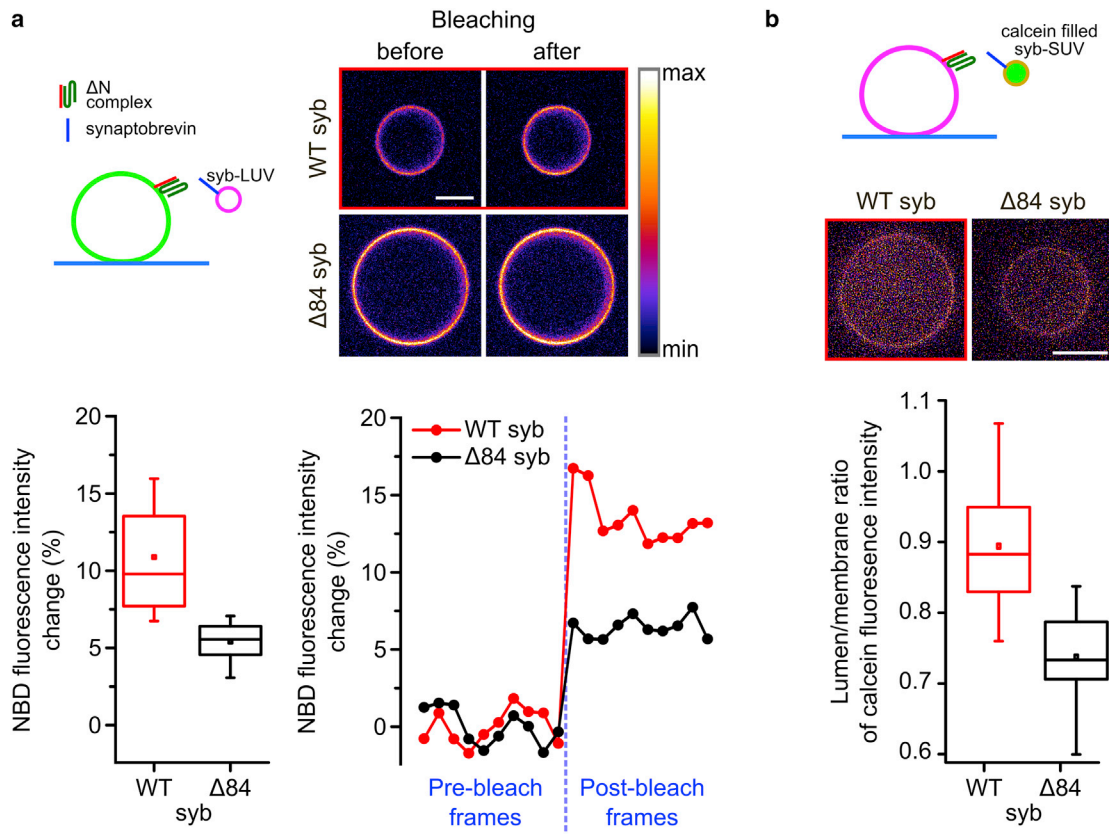
FIGURE 2 SNARE acceptor complex reconstituted into GUVs induces fusion with synaptobrevin-containing liposomes. (*a*) (*Upper panel*) Microscopy images showing ΔN-GUVs containing NBD-PE after ~30 min incubation with LUVs labeled with Rho-PE containing either WT syb (*upper row*) or Δ84 syb (*lower row*) before or after Rhodamine bleaching. Scale bar: 5 μm; lookup table for fluorescence intensities is on the right. (*Lower panel*) Quantification of donor (NBD) fluorescence after acceptor (Rho) bleaching is shown. (*Left*) The box plot shows change of the donor fluorescence intensity after the bleach (*n* = 23 and 16 for WT and Δ84 syb, respectively). Boxes represent interquartile range, and whiskers below and above indicate full data range. Line in a box represents median and square point represents the mean. (*Right*) Fluctuations of donor fluorescence in the GUV membrane before and after bleaching, shown in a representative experiment. (*b*) (*Upper panel*) Microscopy images showing calcein fluorescence of ΔN-GUVs after 30 min incubation in the presence of WT or Δ84 syb-SUVs filled with calcein. Scale bar: 5 μm. (*Lower panel*) Quantification of calcein fluorescence in the lumen of the GUVs, normalized to the membrane fluorescence. Upon docking, calcein fluorescence is restricted to the surface of the GUV, whereas upon fusion the fluorescence intensity of the lumen increases at the expense of that of the membrane (for an explanation of the box plots, see *a*; *n* = 19 and 12 for WT and Δ84 syb, respectively).

Chromaffin granule purification and labeling

Chromaffin granules were purified from bovine adrenal glands using continuous sucrose gradient centrifugation as described in Park et al. ([32](#)). Purified granules were labeled by adding a small aliquot to a dried lipid film consisting of TR-PE and subsequent incubation (30 min, 37°C shaking).

Code availability

Computer code used for generation of linearized membrane intensity profiles, analysis of FRAP data, and dye diffusion simulations (see Supporting Material) is available online (http://dx.doi.org/10.5281/zenodo.376618; http://dx.doi.org/10.5281/zenodo.376619; http://dx.doi.org/10.5281/zenodo.376620).

RESULTS

GUVs containing a reconstituted SNARE acceptor complex (later referred to as ΔN) consisting of syntaxin 1A, SNAP-25A, and a short synaptobrevin fragment (49–96; ([20](#))) and a lipid mix resembling neuronal membranes were immobilized on a functionalized glass coverslip. Fusion of smaller vesicles added in a suspension was monitored around the equatorial plane of the GUV. Interaction of the GUV with the glass surface was limited to the small adherent proportion of the membrane at the bottom of the GUV.

Efficient generation of GUVs containing fusion-active ΔN complexes

GUVs with reconstituted protein were prepared by drying SUVs containing ΔN complex, followed by rehydration and electroformation. The efficiency of protein reconstitution was assessed by measuring the membrane fluorescence intensity of GUVs containing fluorescently labeled ΔN complex and comparing it to the fluorescence intensity of ΔN-GUVs containing fluorescent lipids (see Materials and

Methods; Figs. 1 *a* and S2 *a*; (26)). The optimized GUV-formation procedure led to highly efficient reconstitution (expected concentration 0.1 mol %, i.e., recovery at ~100%) of the ΔN complex in the GUV membrane (Fig. 1 *a*, for GUV diameter distribution see Fig. S1). The lateral mobility of the reconstituted complex was tested with FRAP, yielding a diffusion coefficient that is slightly lower than that of GUV-lipids (Figs. 1 *b* and S2 *b*).

Next, we examined whether the SNARE-GUVs can fuse with liposomes reconstituted with synaptobrevin. For monitoring fusion, we used both a lipid mixing (Fig. 2 *a*) and a content mixing assay (Fig. 2 *b*). Lipid mixing was monitored using an assay involving FRET between labeled membrane lipids. Large unilamellar liposomes (LUVs) containing synaptobrevin and 1.5 mol % of Rhodamine-PE (FRET acceptor) were incubated with ΔN-GUVs containing 1.5 mol % of NBD-PE (FRET donor). Fusion results in mixing of both dyes leading to FRET. Here we assayed for FRET by monitoring the increase of donor fluorescence after photobleaching of the acceptor (Fig. 2 *a*, *lower panel*). FRET was substantially higher when fusion-competent LUVs (containing wild-type synaptobrevin) were used (Fig. 2 *a*, *red points*). In contrast, the increase in the donor signal was lower when a synaptobrevin mutant was used (Δ84 syb) that was previously shown to result in an arrest at the docked state (Fig. 2 *a*, *black points*; (6)).

For content mixing, syb-SUVs were filled with self-quenching concentrations of calcein during reconstitution. Upon fusion of calcein-containing SUVs with a GUV, the dye is rapidly diluted into the large internal volume of the GUV, resulting in fluorescence increase due to dequenching. Here we measured the mean fluorescence intensity of luminal and membrane-localized calcein ~30 min after initiation of the fusion reaction. Addition of fusion-competent SUVs containing WT syb resulted in higher luminal calcein staining than addition of docking-arrested SUVs containing Δ84 syb (Fig. 2 *b*).

Observation of single vesicle docking and fusion events

In the next experiments we took advantage of our system to monitor docking and fusion at the single vesicle level. First, we observed LUVs containing Δ84 syb, which, as described above, are arrested in a docked state after membrane binding. As shown in Fig. 3 *a*, these vesicles were visible as brightly fluorescent spots attached to the GUV membrane. The spots usually diffused on the GUV surface, thus showing high lateral mobility of the docking-arrested SNARE complexes in the plane of the GUV membrane. Notably, vesicles reaching the surface of the coverslip became immobile. This adherence is most probably due to nonspecific adhesion between the surface and the LUV membrane, which occurs despite the hydrophilic nature and the hydrophilic functionalization of the coverslip surface (Fig. S3; and see also Discussion).

Next, we used LUVs containing WT syb that allowed for observing fusion of single vesicles with GUV membranes. Due to the usage of a fast confocal microscope, the time course was resolved with millisecond kinetics. First, we monitored fusion by lipid mixing using GUVs containing the membrane dye DiO and LUVs containing DiD. Fusion was observed by the sudden and rapid dilution of the LUV membrane dye into the GUV membrane (see image sequence in Figs. 3 *b* and S6 *a*). LUV docking and fusion was often visible in consecutive imaging frames. The average delay time between the initial docking and the onset of fusion was determined as 34.8 ± 2.5 ms (mean ± SE, Fig. 3 *c*).

Finally, we monitored single vesicle fusion events using a content release assay similar to that described above except that here another dye (sulforhodamine B) was loaded into syb-SUVs during reconstitution at self-quenching concentrations. Fluorescent bursts were observable just below the GUV membrane surface (Figs. 3 *d* and S7), which resulted from content release of single SUVs. The bursts were short-lived (usually observed in 1–3 imaging frames) due to rapid dilution of the dye into the interior volume of the GUV.

Purified chromaffin granules fuse with ΔN-GUVs with only short delay after docking

Finally, we used the assay for monitoring fusion of chromaffin granules purified from bovine adrenal glands that were shown previously to undergo fusion with SNARE-containing acceptor liposomes (32). These vesicles contain endogenous synaptobrevin 2 along with other proteins important for regulated exocytosis such as Ca^{2+} sensor synaptotagmin 1 (32,33). Purified chromaffin granules were labeled using a dye-coupled lipid (TR-PE) and added instead of liposomes to immobilized GUVs. Chromaffin granules readily attached and fused with ΔN-GUVs (Fig. 4 *a*). Fusion was observable with only short delay after docking (sometimes docking and labeling of the GUV membrane with TR-PE occurring after fusion were observed in subsequent frames). A closer analysis of the delay between docking and fusion revealed at least three kinetically distinct pools of vesicles (Fig. 4 *b*). The fast pool containing 81% of the vesicle population fused on average after 51.6 ± 3.8 ms (mean ± SE) and with a time constant of ~60 ms, the intermediate pool including 14% of the population exhibited an average delay between docking and fusion of 161.3 ± 4.7 ms, and the slowest pool (5% population) fused to GUVs with delay times above 300 ms (Fig. 4, *b* and *c*).

DISCUSSION

Fusion of single vesicles in vitro can be monitored by microscopy using either planar membranes deposited on functionalized surfaces or surface immobilization of small vesicles (see, e.g., (12–19)). While widely used, a problem of these assays that needs to be overcome is that surface contact
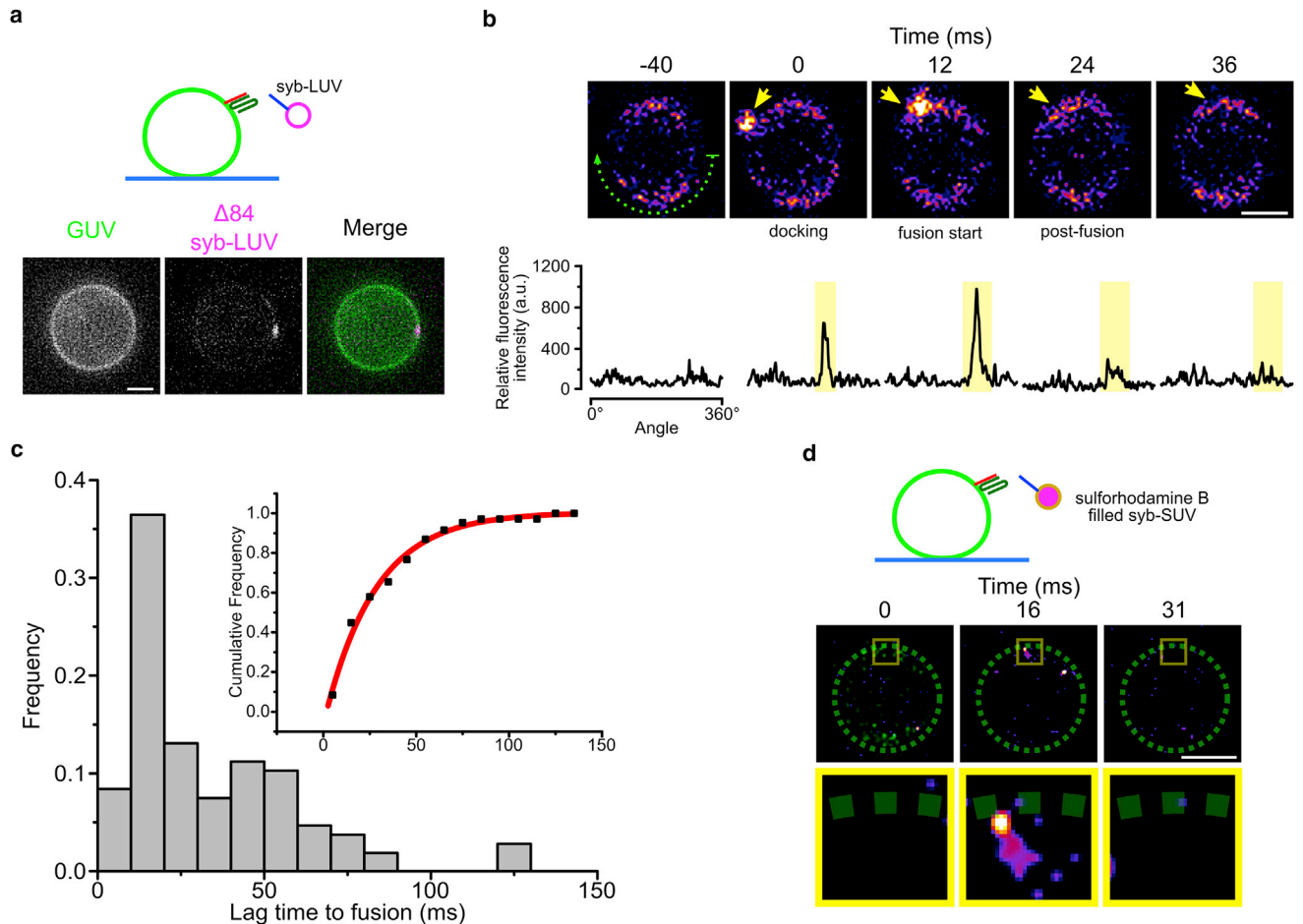
FIGURE 3 Docking and fusion of single liposomes to ΔN-GUVs. (*a*) Single LUV (containing Δ84 syb and labeled with TR-PE, *magenta* on the merged image) bound to the ΔN-GUV membrane labeled with Oregon Green 488-PE (*green* on the merged image). Scale bar: 3 μm. (*b*) Image sequence shows an example of a docked LUV (labeled with DiD and indicated with *yellow arrow*) that fuses with the ΔN-GUV (labeled with DiO, here DiO channel not shown). Scale bar: 1 μm. The fluorescence intensity profiles below the images were obtained from an ~0.6-μm-thick segment of the GUV circumference (*green dotted arrow* indicates line profile start and direction; for details, refer to Fig. S5). Fusion is indicated by a transient increase of fluorescence intensity (12 ms), followed by rapid decay, accompanied by spatial broadening of the signal. Further examples are presented in Fig. S6 and Movie S1. (*c*) Histogram of the lag times between docking and fusion of syb-LUVs (107 fusion events, bin size = 10 ms). (*Inset*) Cumulative frequency distribution of the lag times shown in the histogram. The red curve represents a fit with a first-order kinetic model (see Materials and Methods), resulting in a time constant $\tau = 32.9 \pm 3.5$ ms (value ± SE). (*d*) Image sequence showing a burst of sulforhodamine B fluorescence directed toward the GUV lumen, which results from fusion of a syb-SUV filled with sulforhodamine B at self-quenching concentration. For clarity, the outline of the GUV (detected in another channel and shown as merged image at time 0 ms) is indicated by a green dashed line. Scale bar: 1 μm. (*Lower panel*) Higher magnification of the boxed area in the upper panel is given. Further examples are presented in Fig. S7.

inevitably restricts free lateral diffusion of membrane proteins and lipids, which on the other hand is crucial for fusion to proceed in an unrestricted manner. Various approaches were taken to minimize artifacts contributed by such adhesive interactions such as surface functionalization with hydrophilic molecules minimizing friction (12) or use of porous substrates yielding adhesion-free membrane areas suspended across the pores (14). Here we have employed GUVs with low intrinsic membrane curvature, allowing for monitoring individual fusion events on a free-standing and largely tension-free membrane with high temporal and spatial resolution. Indeed, we observed that the SNARE acceptor complex used was twice as mobile in the GUV

membrane as in supported membrane bilayers (34) whereas the diffusion coefficient measured for labeled membrane lipids was similar to other reports using GUVs (Fig. 1 *b*; and see, e.g., (35)). It needs to be mentioned that the three-dimensional arrangement of the GUV membrane surface makes data acquisition and analysis challenging, particularly when considering that between docking and fusion, vesicles tend to diffuse rapidly across the GUV surface.

Restricting the analysis to the free-standing part of the membrane avoids the docking and fusion reactions being compromised by diffusional constraints or local membrane distortions. Indeed, we observed that within minutes vesicles became trapped at the bottom due to surface adhesion
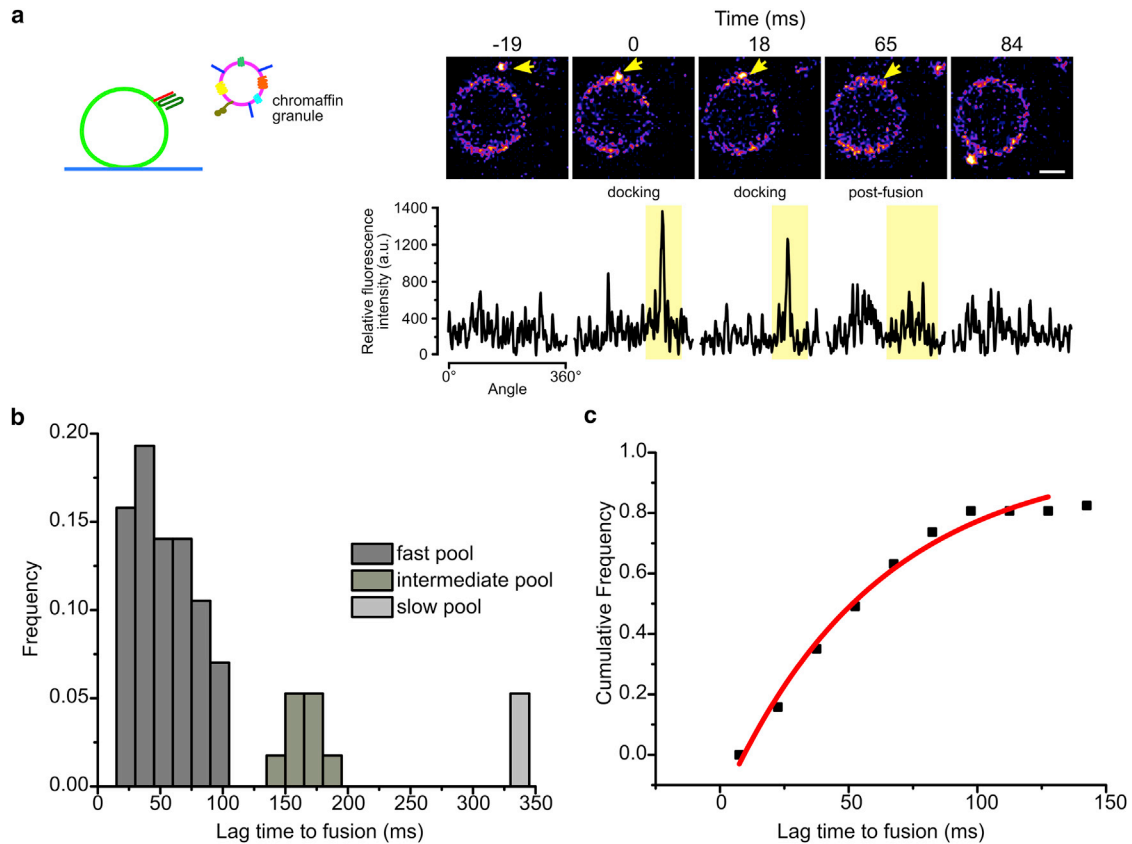
FIGURE 4 Docking and fusion of individual purified chromaffin granules with ΔN-GUVs at high time resolution. (*a*) Image sequence showing a chromaffin granule (labeled with TR-PE and indicated with *yellow arrow*) docking and then fusing with the ΔN-GUVs (visible by a weak labeling in TR channel). Initial TR fluorescence in the GUV membrane is due to fusion events of granules occurring before image acquisition. Scale bar: 1 *μ*m. The fluorescence intensity profiles below the images were obtained by a line scan of the GUV circumference as described in Fig. S5 *a*. See also Movie S2. (*b*) Histogram of the lag times between docking and fusion of chromaffin granules (57 fusion events, bin size = 15 ms). (*c*) Cumulative frequency distribution of the lag times of the fast pool shown in (*b*) (46 fusion events). The red curve represents a fit with a first-order kinetic model (see Materials and Methods), resulting in a time constant $\tau = 60.2 \pm 10.9$ ms (mean $\pm$ SE).

(see Fig. S3). It is conceivable that such adhesion is more prevalent in assays involving immobilized small vesicles with diameters below the resolution limit of the microscope (17,18).

Intriguingly, the delay time between docking and fusion of both liposomes and chromaffin granules was very short, with a substantial proportion of the vesicles showing delays at or below our time resolution of 12 ms. This is remarkable when considering that neither Ca^{2+} nor phosphatidylinositol 4,5-bisphosphate were present, which were shown previously to enhance in vitro fusion (32). In fact, the delay is in a similar range as that observed in intact chromaffin cells between calcium triggering and fusion as measured with capacitance patch-clamping (36). Similarly short delay times were observed previously using small vesicles (liposomes or purified synaptic vesicles) and planar-supported bilayers (12,31). We assume that the activated acceptor complex used here (20) bypasses regulatory steps operating under physiological conditions. Thus, activated SNAREs, without any cofactors, are capable of catalyzing millisecond-rate fusion not only with small vesicles but also with native large secretory granules

despite the presence of an inhibitory peptide in the C-terminal region of the SNARE acceptor complex. Taken together, these findings provide proof of principle that SNARE-mediated fusion can be completed with only millisecond delay time after the initial *trans*-contact of the SNAREs, thus obviating the need to invoke intermediate states with SNAREs arrested at a partially zippered state solely to explain the fast fusion kinetics of neurons (see (3) for a discussion).

In summary, our fusion assay provides, to our knowledge, a new platform for studying membrane fusion on single vesicle level by using an acceptor membrane that is largely free of curvature stress and avoids adhesion-induced artifacts. Furthermore, it can be easily adapted to work with other fusogens such as endosomal SNARE proteins or viral fusion proteins.

SUPPORTING MATERIAL

AUTHOR CONTRIBUTIONS

ACKNOWLEDGMENTS

SUPPORTING CITATIONS

References (37–39) appear in the Supporting Material.

REFERENCES

1. Jahn, R., and R. H. Scheller. 2006. SNAREs—engines for membrane fusion. *Nat. Rev. Mol. Cell Biol.* 7:631–643.

2. Wickner, W. 2010. Membrane fusion: five lipids, four SNAREs, three chaperones, two nucleotides, and a Rab, all dancing in a ring on yeast vacuoles. *Annu. Rev. Cell Dev. Biol.* 26:115–136.

3. Jahn, R., and D. Fasshauer. 2012. Molecular machines governing exocytosis of synaptic vesicles. *Nature.* 490:201–207.

4. Rizo, J., and T. C. Südhof. 2012. The membrane fusion enigma: SNAREs, Sec1/Munc18 proteins, and their accomplices—guilty as charged? *Annu. Rev. Cell Dev. Biol.* 28:279–308.

5. Weber, T., B. V. Zemelman, …, J. E. Rothman. 1998. SNAREpins: minimal machinery for membrane fusion. *Cell.* 92:759–772.

6. Hernandez, J. M., A. Stein, …, R. Jahn. 2012. Membrane fusion intermediates via directional and full assembly of the SNARE complex. *Science.* 336:1581–1584.

7. Tareste, D., J. Shen, …, J. E. Rothman. 2008. SNAREpin/Munc18 promotes adhesion and fusion of large vesicles to giant membranes. *Proc. Natl. Acad. Sci. USA.* 105:2380–2385.

8. Malsam, J., D. Parisotto, …, T. H. Söllner. 2012. Complexin arrests a pool of docked vesicles for fast Ca^{2+}-dependent release. *EMBO J.* 31:3270–3281.

9. Nickel, W., T. Weber, …, J. E. Rothman. 1999. Content mixing and membrane integrity during membrane fusion driven by pairing of isolated v-SNAREs and t-SNAREs. *Proc. Natl. Acad. Sci. USA.* 96:12571–12576.

10. McIntyre, J. C., and R. G. Sleight. 1991. Fluorescence assay for phospholipid membrane asymmetry. *Biochemistry.* 30:11819–11827.

11. Cypionka, A., A. Stein, …, P. J. Walla. 2009. Discrimination between docking and fusion of liposomes reconstituted with neuronal SNARE-proteins using FCS. *Proc. Natl. Acad. Sci. USA.* 106:18575–18580.

12. Domanska, M. K., V. Kiessling, …, L. K. Tamm. 2009. Single vesicle millisecond fusion kinetics reveals number of SNARE complexes optimal for fast SNARE-mediated membrane fusion. *J. Biol. Chem.* 284:32158–32166.

13. Karatekin, E., J. Di Giovanni, …, J. E. Rothman. 2010. A fast, single-vesicle fusion assay mimics physiological SNARE requirements. *Proc. Natl. Acad. Sci. USA.* 107:3517–3521.

14. Schwenen, L. L. G., R. Hubrich, …, C. Steinem. 2015. Resolving single membrane fusion events on planar pore-spanning membranes. *Sci. Rep.* 5:12006.

15. Bowen, M. E., K. Weninger, …, S. Chu. 2004. Single molecule observation of liposome-bilayer fusion thermally induced by soluble *N*-ethyl maleimide sensitive-factor attachment protein receptors (SNAREs). *Biophys. J.* 87:3569–3584.

16. Fix, M., T. J. Melia, …, S. M. Simon. 2004. Imaging single membrane fusion events mediated by SNARE proteins. *Proc. Natl. Acad. Sci. USA.* 101:7311–7316.

17. Diao, J., Z. Su, …, T. Ha. 2010. A single-vesicle content mixing assay for SNARE-mediated membrane fusion. *Nat. Commun.* 1:54.

18. Kyoung, M., Y. Zhang, …, A. T. Brunger. 2013. Studying calcium-triggered vesicle fusion in a single vesicle-vesicle content and lipid-mixing system. *Nat. Protoc.* 8:1–16.

19. Yoon, T.-Y., B. Okumus, …, T. Ha. 2006. Multiple intermediates in SNARE-induced membrane fusion. *Proc. Natl. Acad. Sci. USA.* 103:19731–19736.

20. Pobbati, A. V., A. Stein, and D. Fasshauer. 2006. N- to C-terminal SNARE complex assembly promotes rapid membrane fusion. *Science.* 313:673–676.

21. Margittai, M., D. Fasshauer, …, R. Langen. 2001. Homo- and hetero-oligomeric SNARE complexes studied by site-directed spin labeling. *J. Biol. Chem.* 276:13169–13177.

22. Schuette, C. G., K. Hatsuzawa, …, R. Jahn. 2004. Determinants of liposome fusion mediated by synaptic SNARE proteins. *Proc. Natl. Acad. Sci. USA.* 101:2858–2863.

23. Bacia, K., C. G. Schuette, …, P. Schwille. 2004. SNAREs prefer liquid-disordered over "raft" (liquid-ordered) domains when reconstituted into giant unilamellar vesicles. *J. Biol. Chem.* 279:37951–37955.

24. Angelova, M. I., S. Soléau, …, P. Bothorel. 1992. Preparation of giant vesicles by external AC electric fields. Kinetics and applications. *In* Trends in Colloid and Interface Science VI. C. Helm, M. Lösche, and H. Möhwald, editors. Steinkopff, Heidelberg, Germany, pp. 127–131.

25. Schindelin, J., I. Arganda-Carreras, …, A. Cardona. 2012. Fiji: an open-source platform for biological-image analysis. *Nat. Methods.* 9:676–682.

26. Aimon, S., J. Manzi, …, G. E. S. Toombes. 2011. Functional reconstitution of a voltage-gated potassium channel in giant unilamellar vesicles. *PLoS One.* 6:e25529.

27. Lira, R. B., R. Dimova, and K. A. Riske. 2014. Giant unilamellar vesicles formed by hybrid films of agarose and lipids display altered mechanical properties. *Biophys. J.* 107:1609–1619.

28. Eaton, J. W., D. Bateman, …, R. Wehbring. 2015. GNU Octave Version 4.0.0 Manual: A High-level Interactive Language for Numerical Computations. Free Your Numbers. https://www.gnu.org/software/octave/octave.pdf.

29. Soumpasis, D. M. 1983. Theoretical analysis of fluorescence photobleaching recovery experiments. *Biophys. J.* 41:95–97.

30. Bastiaens, P. I. H., and T. M. Jovin. 1998. Fluorescence resonance energy transfer microscopy. *In* Cell Biology: A Laboratory Handbook. J. E. Celis, editor. Academic Press, New York, NY, pp. 136–146.

31. Kiessling, V., S. Ahmed, …, L. K. Tamm. 2013. Rapid fusion of synaptic vesicles with reconstituted target SNARE membranes. *Biophys. J.* 104:1950–1958.

32. Park, Y., J. M. Hernandez, …, R. Jahn. 2012. Controlling synaptotagmin activity by electrostatic screening. *Nat. Struct. Mol. Biol.* 19:991–997.

33. Wegrzyn, J. L., S. J. Bark, …, V. Hook. 2010. Proteomics of dense core secretory vesicles reveal distinct protein categories for secretion of neuroeffectors for cell-cell communication. *J. Proteome Res.* 9:5002–5024.

34. Wagner, M. L., and L. K. Tamm. 2001. Reconstituted syntaxin1a/SNAP25 interacts with negatively charged lipids as measured by lateral diffusion in planar supported bilayers. *Biophys. J.* 81:266–275.

35. Pincet, F., V. Adrien, …, D. Tareste. 2016. FRAP to characterize molecular diffusion and interaction in various membrane environments. *PLoS One.* 11:e0158457.

36. Voets, T. 2000. Dissection of three Ca^{2+}-dependent steps leading to secretion in chromaffin cells from mouse adrenal slices. *Neuron.* 28:537–545.

37. Eaton, J. W., D. Bateman, …, R. Wehbring. 2016. GNU Octave Version 4.2.0 Manual: A High-level Interactive Language for Numerical Computations. Free Your Numbers. https://www.gnu.org/software/octave/doc/octave-4.2.0.pdf.

38. Wiederhold, K., and D. Fasshauer. 2009. Is assembly of the SNARE complex enough to fuel membrane fusion? *J. Biol. Chem.* 284:13143–13152.

39. Wiederhold, K., T. H. Kloepper, …, D. Fasshauer. 2010. A coiled coil trigger site is essential for rapid binding of synaptobrevin to the SNARE acceptor complex. *J. Biol. Chem.* 285:21549–21559.